Methanol Conversion to Hydrocarbons (MTH) Over H-ITQ-13 (ITH) Zeolite

Methanol Conversion to Hydrocarbons (MTH) Over H-ITQ-13 (ITH) Zeolite

Wegard Skistad • Shewangizaw Teketel • Francesca Lønstad Bleken • Pablo Beato • Silvia Bordiga • Merete Hellner Nilsen • Unni Olsbye • Stian Svelle • Karl Petter Lillerud

Abstract:
Product flexibility is key to meeting fluctuatingcchemicals demands in the future. In this contribution, the methanol to hydrocarbons (MTH) reaction was investigated over two Ge-containing H-ITQ-13 samples, one with needlelike (H-ITQ-13(N), with (Si+Ge)/Al) = 42) and another with plate-like (H-ITQ-13(P), with (Si+Ge)/Al[100) morphology. The samples were characterised using XRD, BET, SEM/EDS and FTIR spectroscopy, and their MTH performance was compared with the performance of H-ZSM-5 and H-ZSM-22. Similar specific surface areas (413 and 455 m2 g-1 for H-ITQ-13(N) and (P), respectively) and similar acid strength (Δν = -327(-310) cm-1) was observed for the two H-ITQ-13 samples. Testing of H-ITQ-13(N) at weight hourly space velocity (WHSV) = 2–8 h-1 at 350–450 C° revealed that C5+ alkenes were the main products (35–45 % selectivity at 400 C°), followed by propene and butene. A low but significant selectivity for aromatic products was observed (6–8 % selectivity at 400 C°). Product selectivity was found to be independent of deactivation. The methanol conversion capacity of H-ITQ-13(N) was 120–150 g methanol g-1 catalyst at 400 C°. Testing H-ITQ-13 at high (30 atm) and ambient pressure, respectively, at 350 C° showed that a high pressure led to enhanced C5+ selectivity, but close to a tenfold decrease in methanol conversion capacity. H-ITQ-13(P) was tested at 400 C° and 2 h-1. It gave lower conversion than H-ITQ 13(N). Furthermore, when compared at the same conversion level, H-ITQ-13(P) gave higher C5+ alkene selectivity, lower aromatics selectivity, and a higher propene to ethene ratio than H-ITQ-13(N). The H-ITQ-13 samples yielded a product spectrum intermediate of H-ZSM-22 and H-ZSM-5. The effluent product cut-off of H-ITQ-13 was similar to that of H-ZSM-5 with tetramethylbenzene as the largest significant product, while H-ZSM-22 produced mainly linear and branched alkenes. The lifetime of H-ITQ-13(N) was clearly enhanced compared to H-ZSM-22, but inferior to H ZSM-5.

Keywords: Methanol; Zeolites ; Hydrocarbons ; MTH; H-ITQ-13

1 Introduction

1.1 Targeted Process

The demand for energy, transportation fuels and plastic raw materials is increasing. Currently, improved living standards in many of the developing countries and rapid population growth are adding up to the high consumption of energy and products taking place in the developed countries. Despite the discoveries of new oil reserves the high consumption and the environmental constraints call for alternative and supporting sources. Upgrading of biomass, coal or natural gas to high value products are all possible supplements to the oil based processes. Recently Shell completed the world's largest gas to liquids (GTL) plant based on Fischer–Tropsch chemistry, in which natural gas (or other carbons sources) is converted to syngas (CO+H2) and further to wax over a cobalt based catalyst before it is cracked into liquids [1]. The product is mainly diesel for the transport sector. An alternative process to the Fischer–Tropsch based GTL process is to synthesise methanol from syngas and then convert methanol to C2+ hydrocarbons, a process known as the methanol to hydrocarbons (MTH) process. It was originally the work of Chang and Silvestri [2], seeking to make high octane gasoline from methanol and isobutane, which led to the discovery of the MTH process in the 1970s. Surprisingly isobutane was not consumed, however; alkenes and aromatics with high octane numbers were still formed. The only explanation to this observation was that the products originated from methanol [2–4]. Following their discovery an MTH plant, based on natural gas as raw material, was built in New Zealand and optimized to produce hydrocarbons in the gasoline range, yielding about 80 % selectivity towards C5+ from syngas (the so-called methanol to

gasoline (MTG) process) [5]. However, due to falling oil prices the MTG part of the plant was closed in the mid 1990s [5]. Today the oil prices are again high and the MTH process has gained renewed focus. The MTH process takes place over zeolites, which are porous crystalline aluminiumsilicates. They represent one of the most important families of heterogeneous catalysts as they possess unique shape selective properties arising from the molecularly sized, regular pore system with strong Brønsted acid sites exposed to channels and cavities. Within these pores, the MTH reaction proceeds via a complex inorganic–organic reaction network which has been thoroughly studied in academia and in industries. The mechanistic understanding of the MTH reaction has evolved over the past 30–35 years. Soon after its discovery it was suggested that the MTH reaction is autocatalytic [6]. Still, the majority of early reaction studies focused on the formation of the first C–C bond from two methanol molecules, and more than 20 versions of this direct mechanism were proposed [3]. Later, substantial evidence was found for the existence of an indirect mechanism under steady state conditions [7–12]. In this mechanism, various hydrocarbons, denoted the ‘‘hydrocarbon pool’’, have been found to act as autocatalytic species. Today, it is generally acknowledged that the hydrocarbon pool mechanism dominates under steady-state conditions, mainly due to the substantially higher activation energies for the direct C–C formation from C1 entities compared to methylation and cracking of higher hydrocarbons, but also due to the observation of an induction period of increasing conversion in certain catalysts, before it reaches a steady state activity. However, the induction period and the initial C–C bond formation are still debated and not clearly known [13]. Product selectivity is to a large extent determined by shape selectivity in the MTH reaction. Product shape selectivity [14] was demonstrated by the cut-off in products observed over zeolites with various channel size; from light linear alkenes in H-SAPO-34, via branched alkenes in H-ZSM-22, to tetra-methylbenzene in H-ZSM-5, and hexamethylbenzene (hexaMB) in H-beta zeolite [5]. Intermediate shape selectivity has been demonstrated by mechanistic studies aimed at elucidating the active hydrocarbon pool species in various zeolite topologies. Steady-state isotopic transient experiments have been widely used for this purpose. In wide-cavity and wide-channel H-SAPO-34 and H-beta, respectively, the main reaction centers have been identified as hexaMB and heptamethylbenzenium cation, which may both be converted to alkenes and the corresponding lighter polymethylated benzene analogues [15–19]. In intermediate-channel H-ZSM-5, C3+ Aliene and lighter polymethylbenzenes (triMB and tetraMB in particular) were found to act side by side as hydrocarbon pool species, leading to light alkene formation through consecutive methylation and dealkylation reactions. In H-ZSM-5, ethene was found to originate mainly from polyMB intermediates [20–26]. Later, a comparative study between H-ZSM-5 and H-beta zeolite as MTH catalysts revealed that ethene and propene were main products from the light polyMBs present in H-ZSM-5, while propene and isobutane were the main products from the heavier poly-MBs which dominated in wide-channel H-beta zeolite [23]. Further exploration of a unidirectional zeolite H-ZSM-22 with slightly smaller pore size than H-ZSM-5 showed that alkenes were the dominating intermediates in this topology. In accordance with the findings over H-ZSM-5, ethene formation was insignificant over H-ZSM-22 [27]. The impact of channel size on product selectivity is reflected in the industrial use of zeolite and zeotype catalysts. Medium size pore H-ZSM-5 (ten-ring, three dimensional channels of size 5.4 9 5.6 and 5.3 9 5.5 A °) is the working catalyst in MTG and the related Topsøe integrated gasoline synthesis process [28], while the closely related UOP/hydro methanol to olefins (MTO) process producing light alkenes uses the small pore H-SAPO-34 (eight-ring, three dimensional cavity structure with window size of 3.8 9 3.8 A°) [29]. Another important industrial process is the methanol to propene process developed by Lurgi [30]. Also here H-ZSM-5 works as a catalyst, although theconditions are optimized for propene production. The latter example demonstrates that parameters other than cavity and channel size, such as reaction conditions, acid site density, acid strength, crystal size and morphology, defects and eventually coke formation, can significantly influence product selectivity [5]. Such effects have been most widely studied for the H-ZSM-5 topology, and a few examples will be cited here. The effect of acid site density on the selectivity in MTH over H-ZSM-5 was reported by

Chang et al. and Prinz and Riekert [31–33]. Both found that a reduced acid site density (increasing Si/Al ratios) led to enhanced alkene selectivity and increased propene to ethene ratios. The same conclusion was reported for decreasing H-ZSM-5 crystal sizes [33]. Both examples are in agreement with the consecutive reaction scheme originally proposed by Chang and Silvestri [2] for the H-ZSM-5 catalyst, where light alkenes are the initial products, which are subsequently converted to alkanes and aromatic products by hydride transfer reactions. Adding the more recent mechanistic insight from isotopic labelling studies, the changes in the propene to ethene ratio with changing acid site density and crystal size could be tentatively ascribed to the relative abundance of the alkene versus the methylbenzene reaction cycle depending on the relative diffusion and reaction rates in the various materials [24–26]. Very recently, a comparison between conventional H-ZSM-5 crystals and nanosheets of only about 4 nm thickness and similar Si/Al ratio, showed strikingly similar product selectivities for the two materials, except for a slightly higher aromatics selectivity for the nanosheet morphology, as well as the propene to ethene ratio, which was significantly higher in the material with nanosheet morphology (42 vs. 12, respectively, at 70 % methanol conversion at 350 C°) [34]. Improved alkene versus aromatics selectivity has also been observed for increasing temperatures [31]. Recently, from comparative tests of a series of different H-ZSM-5 samples, enhanced propene selectivity was ascribed to lower density of strong Brønsted acidic sites, longer diffusion path and lower density of lattice defects [35]. Similar results to those obtained over H-ZSM-5 have been reported for catalysts with MOR topology [36]. Among the main products, ethene, propene and butene; ethene selectivity was found to be much higher for Si/Al ratios in the range 5–12 than in the range 55–103. High propene yield was observed for mordenite samples in the range 12–103 and the butene yield increased with increasing Si/Al ratio. Although much knowledge has been gained about the MTH reaction system and mechanism-topology correlations, some challenges are yet to be solved. Clearly it is important to find new catalysts or modify already known materials to gain flexibility in the product spectrum to meet fluctuations in the future market. Among more specific goals, one is to limit formation of durene (tetraMB) in the MTG process, due to its rather high melting point [5]. Another one is to find catalysts which may selectively form products intermediate of H-SAPO-34 and H-ZSM-5, without compromising on the long life-times observed over H-ZSM-5. In such a perspective the combination of improved reaction rates with shape selectivity from the more than 200 known different zeolite topologies and the many hypothetical frameworks possessing different canne and cavity sizes gives great possibilities regarding the future product spectrum library of shape selective, green catalysis in methanol conversion [37, 38]. 1.2 Material Studied in This Work Zeolites are, according to a strict definition, porous aluminiumsilicates, but materials containing other elements are often counted as zeolites as well. One such example is the Ge containing H-ITQ-13 zeolite whose lattice contains Ge in addition to Al, Si, O and protons. According to previous syntheses of this zeolite and the characterization thereof, Al is difficult to introduce into the structure without the help of Ge stabilizing the strained double four rings found in the structure [39]. In the first published article on H-ITQ-13 the structure was Ge-free and Al was typically introduced by substituting B with Al by post synthesis treatment [39, 40]. The stabilizing effect of Ge has been shown for many other structures containing double four rings and especially interesting is the high stabilizing effect of Ge in double three rings, the latter found to be an important parameter forming extra large pore zeolites with very low frame work density (FD), defined as the number of T-atoms per 1,000 A ° 3, bridging the interesting gap between the microporous and the mesoporous materials [38, 41–44]. H-ITQ-13 is a medium pore size zeolite and it is synthesised by the fluoride route which introduces F-, typically from hydrofluoric acid or ammonium fluoride, into the synthesis mixture. This anion also plays a crucial role since it can go into the space between strained double four rings and [41,52,62]-units and stabilize the structure together with Ge [41]. In H-ITQ-13 about half of the [41,52,62]-units are filled with one F--ion and it has been shown that the double four rings likely contain 2 or 3 Ge atoms preferably as shown in Fig. 1 [45, 46]. Despite the high content of Ge the material has been shown to be stable after calcination at 480 C° in the presence of moisture with Si/Ge ratios as low

as 5 [39]. The topology of H-ITQ-13, ITH, with three differen channels is shown in Fig. 2. This zeolite has one zig-zag ten-ring channel along the crystallographic c-axis of dimension 4.8 9 5.3A°. Such a channel can also be found in the well known catalyst H-ZSM-5 for converting MTG, although the dimensions for the latter are larger than in H-ITQ-13. Another interesting feature is the presence of a straight nine-ring channel in the H-ITQ-13 structure with size of only 4.0 9 4.8 A° . This is a rather rare organization of the pore aperture and it is reasonable to assume that the smaller channel can result in intermediate shape selectivity between 8- (as for MTO, mainly ethene and propene) and ten-ring (as for MTG, mainly C5 hydrocarbons including aromatics) based zeolites. The last channel is a straight ten-ring channel with dimension 4.8 9 5.1 A ° and goes along the crystallographic b-axis.The H-ITQ-13 zeolite therefore has similarities to the H-ZSM-5 catalyst which facilitates gasoline synthesis from methanol, but differs with respect to canne dimensions leaving H-ITQ-13 slightly smaller. From this perspective, H-ITQ-13 was expected to give products in the gasoline (i.e. C5+ hydrocarbons) range, but on the other hand, the slightly smaller canne dimensions was expected to favor a product mixture rich in the smaller hydrocarbons compared to H-ZSM-5. The present work elucidates the effect of the reaction conditions (temperature, flow, ambient and high pressure) on the selectivity of this less studied H-ITQ-13 zeolite, with two sets of acid site density and morphology, in the MTH reaction. Herein we describe detailed synthesis procedures and characterisation results of the H-ITQ-13 materials using X-ray diffraction (XRD), scanning electron microscopy (SEM), N2 sorption measurements and infrared spectroscopy as well as MTH test results.

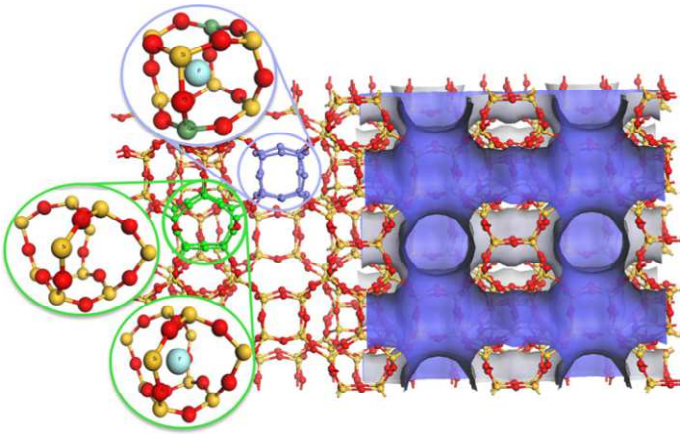

Fig. 1 Structure units stabilized by Ge and or F-. Around half of the [415262]-units are filled with 2–3 Ge atoms in opposite corners are most likely preferred in the double four rings

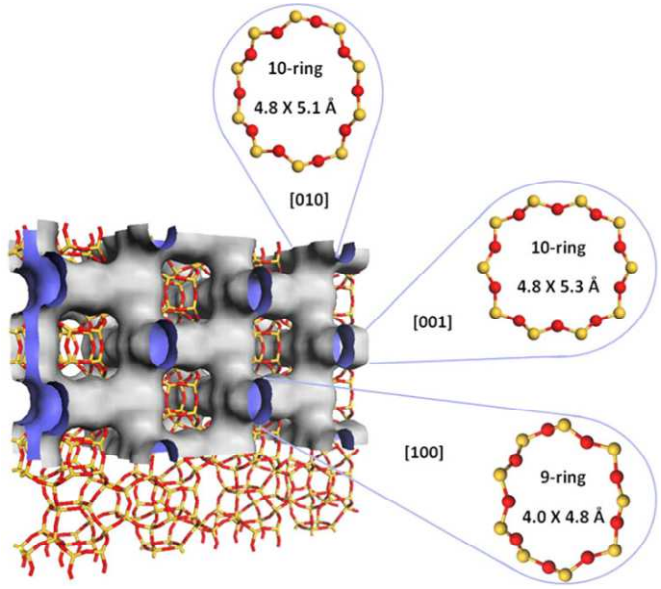

Fig. 2 The channel system and dimensions of the pore apertures in the H-ITQ-13 zeolite. One ten-ring zig-zag channel of dimension 4.8 9 5.3 A° is present along the crystallographic c-axis [001]. There are two more channels, one straight ten-ring canne (4.8 9 5.1 A°), and one straight nine-ring channel (4.0 9 4.8 A°)

2 Experimental

2.1 Synthesis

H-ITQ-13 is typically synthesized by the fluoride route in highly concentrated synthesis mixtures using hexamethonium hydroxide (HM(OH)2) as a structure directing agent (SDA) [39, 40]. The SDA in hydroxide form was premade by dissolving 54 g hexamethonium bromide in water and ion exchanged with 300 g amberlite IRN-78 resin in a column. The template solution was then rotaevaporated to a solution which typically ended up around 20–25 wt% HM(OH)2 in water. The wt% was determined by titration with 0.1 N HCl using BTB as an indicator. The synthesis mixture of ITQ-13(N) was prepared in a plastic beaker by dissolving 0.46 g GeO2 in 11.75 g of 24.5 wt% HM(OH)2 aqueous solution under stirring. Then 0.20 g Al-isopropoxide was dissolved in a small amount of isopropanol, added to the template solution and kept under stirring. Under rapid stirring 9.26 g TEOS was added dropwise. The plastic beaker with the synthesis mixture was weighed and put for stirring for 1–2 h at room temperature. Then the beaker was heated to around 80 C° (while stirring) until all the ethanol (8.18 g), the small amount of isopropoxide and the excess water (2.88 g) had evaporated. The gel turned thick after a while and it was then regularly manually stirred. When all the alcohol and water was evaporated 1.36 g HF (40 wt% in water) was added to the mixture and manually stirred. It then turned into a very dry powder-like mixture. This procedure resulted in a final molar composition of 91 SiO2:1 Al2O3:9 GeO2:56 HF:25 HM(OH)2:500 H2O. Here it is taken into account that every mole of TEOS consumes 2 mol of water and produces 4 mol of ethanol. To the final gel small amounts of pure Si-ITQ-13 seed crystals (see below) were added and the mixture was transferred to 52 ml Teflon liners in a stainless steel autoclave and kept in a tumbling oven (vertical rotation) at 37 rpm for 14 days at 160 C°. Then the autoclaves were quenched and the product was washed several times with distilled water to pH was close to neutral. After drying the product was calcined in 50:50 N2 and O2 for 8 h; 3 h heating from room temperature to 550 C° and at 550 C° for 5 h. In the synthesis of H-ITQ-13(P) the same procedure as H-ITQ-13(N) with nearly identical synthesis composition but 10.7 % less fluoride (50HF instead of 56HF), was followed, but yielded a morphology similar to the aluminium substituted B-ITQ-13 obtained in [39], which was Ge free and had low Al content. In our case EDS analysis and IR showed that Ge and Al were present in H-ITQ- 13(P), but to a much lesser extent than in H-ITQ-13(N) (see Sect. 3.1). Crystal growth may be facilitated by adding seeds, and this is a common procedure for synthesis in fluoride media with highly concentrated gels. In this work pure Si-ITQ-13 was made prior to the synthesis by the same procedure excluding Ge and Al. The synthesis mixture for making seeds had a final molar composition of 100 SiO2:50 HF:25 HM(OH)2:500 H2O. Typically (up to) 0.11 g seeds were added to the recipe for the Al and Ge containing H-ITQ-13 described above to improve nucleation rates and reduce the risk of failed reproduction.

2.2 Characterization of the Material

The crystallinity and purity of the material was determined using XRD. The measurements were performed using a Siemens Bruker D5000 instrument with Bragg–Brentano geometry and Cu Ka1 radiation (k = 1.5406 A°). The size, morphology and the (Si+Ge)/Al ratio of the catalyst particles was determined with SEM. Micrographs were recorded on a FEI Quanta 200 FEG-ESEM equipped with an Everhart–Thornley detector and a EDAX EDS detector. The BET surface area and pore volume were determined using nitrogen physisorption measurement at liquid nitrogen temperature (in a range of relative pressure 0–0.99 P/P0). The sample was outgassed under vacuum for 5 h, 1 h at 80 C° and 4 h at 300 C°, before measuring. The measurements were performed on a Belsorp-mini II instrument. IR measurements were performed on a Bruker Vertex 80 instrument with MCT detector. The sample was pretreated at 120 C° for 1 h, at 350 C° for 1 h and at 450 C° for 1 h under vacuum. CO was used as a probe molecule at liquid nitrogen temperature.

2.3 Catalytic Testing

2.3.1 Ambient Pressure Tests

All ambient pressure catalytic tests were performed with 50 mg sample in a fixed bed quartz reactor with 10 mm inner diameter. The zeolite powder was pressed into wafers and subsequently crushed and sieved to obtain particles in the range 250–420 μm before transferring the catalyst to the reactor. Before all tests the catalysts were calcined in situ in pure oxygen for 1 h at 550 C°. Methanol was fed by passing He through a saturation evaporator (BDH Laboratory Supplies,[99.8 % chemical purity) kept at 20 C°, giving a WHSV in the range of 2–9 g methanol per g of catalyst per hour. The product stream was analyzed using an automatic injection gas chromatograph connected directly to the reactor outlet by a heated transfer line. An Agilent 6890A GC with FID, equipped with a Supelco SPB-5 capillary column (60 m, 0.530 mm i.d. stationary phase thickness 3 lm) was used for the analysis. The temperature of the oven was programmed between 45 and 260 C° with a heating rate of 25 C° min-1 (hold time = 5 min at 45 C° and 16 min at 260 C°).

2.3.2 High Pressure Test

The high pressure catalytic test was performed at 30 bar (regulated using back pressure controller) using 150 mg catalyst (200–420 μm sieved fraction). The catalyst bed was supported using quartz wool plugs on a fixed bed reactor with 4 mm internal diameter. Prior to methanol feed, the catalyst was activated at 500 C°, the reactor was beate (5 C° min^{-1}) under flow of N2 (100 ml min^{-1}) and keep for 2 h under the flow of 2 % O2 in N2 (100 ml min-1). The MTH reaction was performed at 350 C° and WHSV = 2 h-1. Methanol was fed as a liquid using an ISCO high pressure syringe pump. N2 was used as a carrier gas. The total flow of the reaction mixture was 63 ml min-1 (mol% of liquid methanol in the feed = 5.6). The reaction product was analyzed using an online Agilent 7890A gas chromatograph, equipped with Restek Rtx-100-DHA column (100 m, 0.25 mm i.d., 0.5 lm df) and a Restek Rtx-5PONA pre-column (2.5 m, 0.25 mm i.d., 1.0 μm df).

2.4 Analysis of Retained Species

During reaction large hydrocarbons can be trapped inside the zeolite pores. These trapped species were analysed by dissolving 20 mg of used zeolite in a small capped Teflon vial with 1 ml 15 % HF. Addition of 1 ml dichloromethane with hexachloroethane as internal standard allowed extraction of the organic phase for analysis by GC–MS. An Agilent 6890N gas chromatograph connected to an Agilent 5792 mass-selective detector with a HP-5MS column (60 m, 0.25 mm i.d., stationary phase thickness 0.25 lm) was used for the analysis. The temperature of the oven was programmed between 50 and 300 C° with a heating rate of 10 C° min^{-1} (hold time = 3 min at 50 C° and 15 min at 300 C°). The mass spectral library of the NIST98 database was used for identification.

3 Results and Discussion

3.1 Characterization of Materials

3.1.1 XRD, SEM and N2 Sorption Measurements

X-ray diffractograms (XRD) of H-ITQ-13(N) and H-ITQ-13(P) are shown in Fig. 3. They revealed no visible impurities when compared to the calculated diffraction pattern. Pawley refinement showed small variations between 20 and 25 2-theta values caused by small differences in peak position and peak shape. The diffractograms are in agreement with the one published in the original patent [40]. SEM micrographs of H-ITQ-13(N) in Fig. 4 showed needle to rice-like particles which varied in length and thickness, but the majority of the particles were less than 3 lmin length and around 100 nm in width. The particles were thinner than those reported in [39] where thicker needles or rods were observed. EDS analysis gave a (Si+Ge)/Al ratio of (36.91 + 1.49)/0.92 = 42 which is slightly lower than in the synthesis mixture of 50. The BET surface area of H-ITQ-13(N)

was measured to 413 m2 g-1 and the t-plot method showed a micropore volume of 0.15 cm3 g-1 and a mesopore volume of 0.09 cm3 g-1, in agreement with previous literature on H-ITQ-13 [39]. SEM micrographs of H-ITQ- 13(P) showed plate-like crystals which differed from the needle or rise-like particles of H-ITQ-13(N).EDS analysis of H-ITQ-13(P) showed the presence of Ge and Al, but in too low amounts to report a reliable (Si+Ge)/Al ratio. The BET area of H-ITQ-13(P) was 455 m2 g-1 and the micropore volume was 0.15 cm3 g-1, while the mesopore volume was 0.54 cm3 g-1. Based on these findings the two samples have comparable surface areas and pore volumes, but clearly differ with respect to morphology and acid site density.

3.1.2 FTIR

FTIR spectra of H-ITQ-13 with increasing CO doses are shown in Fig. 5. The m(O–H) and the m(CO) regions are shown in the left and right panel, respectively, and the red curve is the activated zeolite without any CO while the blue curve corresponds to the maximum CO adsorption. For H-ITQ-13 we would expect bands of slightly acidic silanol (:Si–OH) and germanol (:Ge–OH) groups and the more acidic Brønsted sites (:Si–(OH)–Al: and :Ge–(OH)–Al:) in the m(O–H) region. Concentrating first on the H-ITQ-13(N) sample (lower panel) and the activated sample (red curve) the band at 3,743 cm-1 is assigned to the fairly isolated silanols mostly located on the external crystal surfaces. Partial extra-framework Al typically shows a band at 3,665 cm-1 and corresponds to the band at 3,667 cm-1. However, previous studies on Ge- ZSM-5 assigned the bands at 3,670 3,680 cm-1 to the corresponding germanols [47].

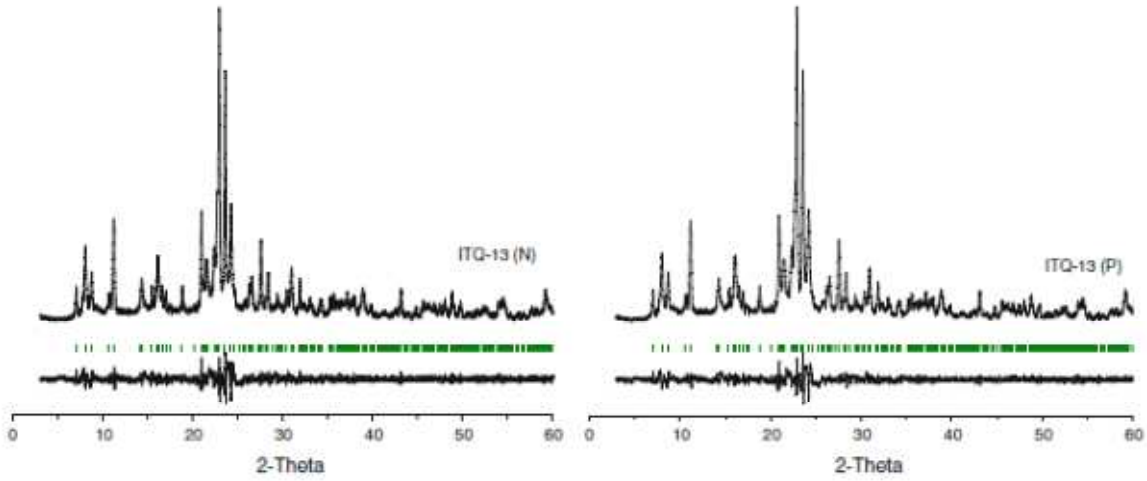

Fig. 3 X-ray diffraction of as synthesised ITQ-13(N) left and ITQ-13(P) right

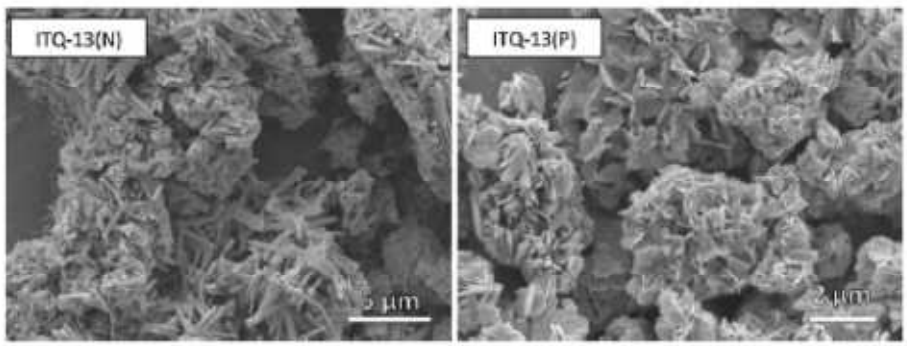

Fig. 4 SEM micrographs showing needle-shaped (ITQ-13N) and nanometer thick platelike (ITQ-13P) crystals of various length

Accordingly, the band observed here at about 3667 cm-1 may be an overlap between the terminating germanol band and eventually partially extra-framework aluminum (as illustrated also

from the shoulder on the perturbed OH-groups from silanols which can be assigned to the germanols, and the perturbed OH groups associated with Al defects upon CO adsorption as described below). The maximum at 3,627 cm-1 (with a tiny shoulder around 3,610 cm-1) can be related to the Brønsted acid sites. FTIR of germanium containing H-ITQ- 7 in [48] showed a clear shoulder at these wavenumbers (3630 cm-1 and 3,610 cm-1) and this was assigned to different crystallographic positions of the :Si/Ge–(OH)– Al: and not to the acid strength difference as two bands also were visible in the pure aluminosilicate H-ITQ-7 [46,48, 49]. The component at 3,564 cm-1, not visible for H-ITQ-7, indicates that H-ITQ-13 has some hydroxyls most probably weakly perturbed by an oxygen of a closeby,zeolitic wall, as already seen in case of other zeolites [50]. The true intensities of all the maxima in the range 3700–3560 cm-1, is not clear as they are emerging from a very broad absorption that extends till 3,200 cm-1, testifying the extended defectivity of this material. At maximum CO coverage (blue curve), most of the hydroxyl species are eroded and red-shifts were observed in the m(O–H) region due to OH–CO interaction. A large portion of H-bonded silanols can be associated with the maximum at 3,649 cm-1 ($\Delta\nu$= -94 cm-1), while in case of germanols the observed shift is not easily quantified, since the unperturbed germanols may overlap with partial extraframework Al. In H-ITQ-7 the germanol band in the activated zeolite at 3679 cm-1 shifted to 3596 cm-1 when CO was adsorbed. In the case of H-ITQ-13 the germanol band was shifted to about 3585 cm-1 while the Brønstedband (-Si/Ge–(OH)–Al-) was shifted from 3627 (or from the shoulder at 3610 cm-1) to 3290 cm-1. Thus theacid strength was calculated from where the band is stabilised (marked with a black dotted line at about 3300 cm-1) giving a shift of $\Delta\nu$ = -327 (or from shoulder -310 cm-1). This shift is comparable to highly acidic materials such as H-ZSM-5, H-ZSM-22 and H-TNU-9 [27,51, 52]. The strong interaction of CO with Brønsted-acid sites resulted in a broad band with a second component centred around 3470 cm-1 commonly assigned to m(O–H) of perturbed OH-groups close to Al defects (partial extraframework Al) [48]

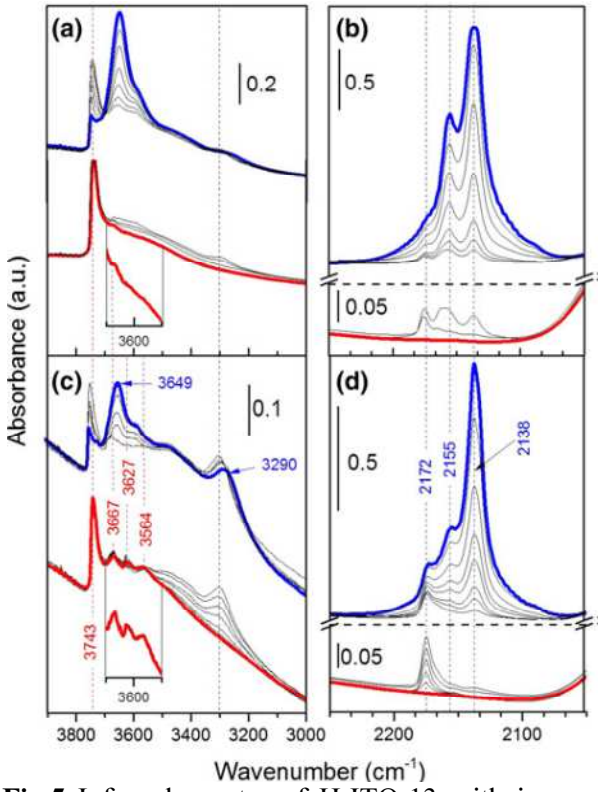

Fig.5 Infrared spectra of H-ITQ-13 with increasing CO dose. Red curve shows the zeolite without CO adsorbed and the blue curve shows the maximum CO adsorption. The m(O–H) region of a H-ITQ- 13(P) and c H-ITQ-13(N) is shown in the left panel while the m(CO) region of b H-ITQ-13(P) and d H-ITQ-13(N) is shown to the right. The small frames in the m(O–H) regions are magnified views of the bands between 3,700 and 3500 cm^{-1} which gave less visible Brønsted-band for H-ITQ-13(P)

In the CO region (right panel), interaction between CO and Brønsted-acid sites leads to donation of electrons (slightly antibonding) on the C to form a weak bond to the H on the site which results in reduced repulsion between the electrons in the CO bond which again reduces the CO bond length. In the right panel this effect can be seen from the band at 2138 cm-1, corresponding to liquid-like CO in the pores interacting with the homopolar hydroxyl free zeolite surface, blue-shifting to 2172 cm-1 when CO interacted with the Brønsted-site as described. Note that the band is strongly asymmetric, indicating the heterogeneity of the interaction sites. The lower electron attraction by silanols and germanols resulted in a smaller shift from 2138 cm-1 to 2155 cm-1. However the change in the CO bond due to interaction with germanols and silanols was not sufficient to be seen as individual bands in the m(CO) region in accordance to what observed for Ge containing H-ITQ-7 [48]. It can also be mentioned that no visible bands at 2,220 cm-1 indicate the absence of strong Lewis acid sites in H-ITQ-13(N). The H-ITQ-13(P) sample (upper panel) showed similar features to the H-ITQ-13(N) sample even if a few major differences are evident: (i) nearly free silanols species are much more abundant than in the previous case (note the scale is nearly doubled) moreover (ii) a much lower density of strong acid sites than in H-ITQ-13(N) was found, in accordance with EDS data. In the OH-region the band at 3630 cm-1 was barely visible for H-ITQ-13(P) in the activated zeolite, but became visible upon CO adsorption both in the OH and CO region (growing bands at 3290 and 2172 cm-1, respectively). Furthermore, a lower Ge content was reflected in a lower abundance of external germanol bands. The undefined broad adsorption, starting as a tail of the free silanols band, extended till 3,200 cm-1, testifying the high defectivity of the material. The hydroxyl groups that originated this band were not affected by CO probing. Conversely, the high amount of free silanols was easily evidenced by the strong component at 2,155 cm-1, due to weakly adsorbed CO. Also for this sample there were no visible bands at 2,220 cm-1 indicating no strong Lewis acid sites in H-ITQ-13(P).

3.2 Catalytic Performance in MTH

3.2.1 Catalytic Testing of H-ITQ-13(N) at Ambient Pressure

Methanol conversion versus time on stream data obtained over H-ITQ-13(N) at 400 C° with WHSV = 2–8 h-1 are shown in Fig. 6. As expected, the initial conversion increased with increasing contact time, reaching 97 % at WHSV = 2 h-1. The conversion versus time on stream curves had an increasingly negative slope with time on stream, typical of the MTH reaction, and characteristic of a catalytic system in which activity and deactivation reactions are both proceeding in a narrow zone of the catalyst bed, gradually progressing towards the end of the catalyst bed with time on stream [5]. Cumulative methanol conversion curves for H-ITQ-13(N) are shown as Supporting Information (Fig. S6). The cumulative methanol conversionmcapacity (i.e. the gram amount of methanol convertedto products per gram catalyst before complete deactivation, which is calculated by integrating the total area under the conversion curve [53] was similar for the three tests, i.e.; 120–150 g methanol g-1 catalyst. Product selectivity (in carbon %) versus conversion graphs for WHSV = 2 h-1 at 400 C° are shown in Fig.7. Concentrating again on the data obtained over H-ITQ 13(N) (closed symbols), C6+ aliphatic products constituted the main product group, closely followed by propene (29 and 28 % selectivity, respectively, at 70 % conversion). Butenes and pentenes (15 and 14 % selectivity, respectively, at 70 % conversion) were the third and fourth largest product groups. Only small amounts of aromatic products (6 % selectivity at 70 % conversion), alkanes (3 % butanes and 2 % methane at 70 % conversion) and ethene (2 % at 70 % conversion) were formed. In total, the typical gasoline product range, i.e. C5+ hydrocarbons, represented 49 % of the products at 70 % conversion, out of which 43 % was non-aromatic C5+ hydrocarbons. Catalytic test data for H-ITQ-13(N) at 350 and 450 C° are shown as Supporting Information (Fig. S9). The trends in conversion and selectivities were similar to those observed at 400 C°, albeit with a tendency of a higher aromatics fraction and less C5 aliphatics for a given conversion, at the lowest temperature, in agreement with thermodynamics [54]. Product yield versus conversion curves for H-ITQ-13(N) at 400 C° and WHSV = 2–8 h-1, obtained during progressive deactivation of the catalyst at each

contact time, are shown in Fig. 8.H-ITQ-13(N) withWHSV = 2 h-1 had been on stream for almost 50 h before it reached the same conversion as the fresh catalyst when the WHSV was 9 h-1. Excellent overlap was observed between data obtained at different contact times and degrees of deactivation for theC2, C3, C4, C5 and C6+ (alkene and alkane) fractions, whereas small deviations were observed for the CH4 and C6+ Aromatics fractions, which both increased in abundance with more deactivation. The yield of each of these products was so small, however, that the differences represented only minor differences in the yields of the remaining products (mainly the C3 and C4 fractions). Overall, the data presented in Fig. 8 suggest that deactivation of H-ITQ-13(N) does not alter effluent product selectivity, and consequently, that selectivity (and yield) versus conversion curves for various samples may be compared by simply performing one experiment for each of them, even if their initial conversion differ. The same conclusion has previously been drawn for the MTH reaction over a range of ten-ring-pore zeolites; i.e. 3D H-ZSM-5 [55], and 1D H-ZSM-22, H-ZSM-23, and H-EU-1 [56]. Amajor consequence of such an observation is that deactivation modeling and single event kinetic modeling of the MTH reaction over H-ITQ-13 zeolites could be achieved by minor modification of models already developed for H-ZSM-5 [57, 58].

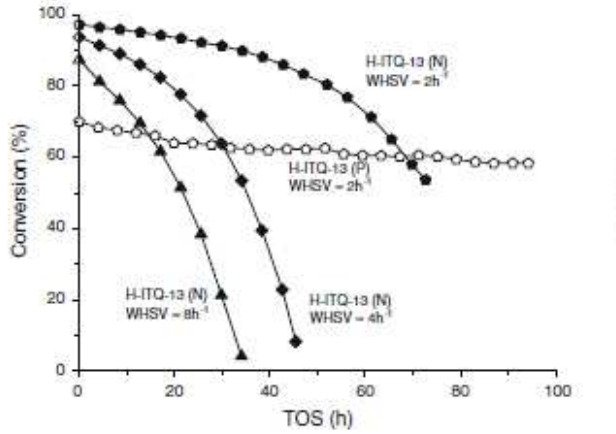

Fig. 6 Methanol conversion (%) versus time on stream (h) for H-ITQ-13(N) at 400 C° and WHSV = 2, 4 and 8 h-1 and for H-ITQ-13(P) at 400 C° and WHSV = 2 h-1

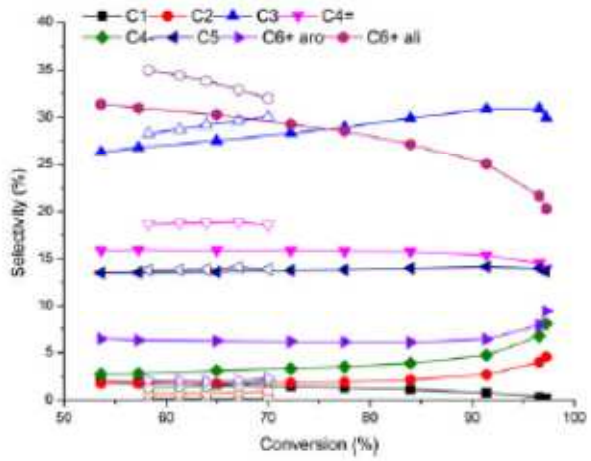

Fig. 7 Product selectivity (%) versus methanol conversion (%) for H-ITQ-13(N) (closed symbols) and H ITQ-13(P) (open symbols) at 400 C° and WHSV = 2 h-1

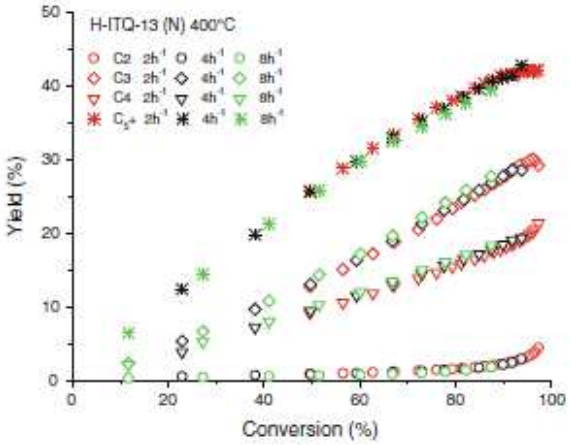

Fig. 8 Product yields (%) versus methanol conversion (%) over H-ITQ-13(N) at 400 C° and at WHSV = 2 (red), 4 (black), 8 (green) and 9 (blue) h^{-1}

Retained hydrocarbons in deactivated H-ITQ-13(N) were analysed with GC–MS after testing at 350–450 C°. The data are shown in Fig. 9. At 350 C°, pentamethylbenzenes (pentaMBs) were the dominating species followed by tetraMBs. Only small amounts of toluene and xylenes were detected among the MBs. The heaviest retained species which were obtained in appreciable amounts were tri- and tetramethylnaphtalenes. A minor peak was visible at 30 min retention time and was identified as tetramethylantracene. Dissolution of the zeolite operated at higher temperatures showed reduction in the amount of hydrocarbons retained, especially with respect to pentaMBs. It should be noted that a decrease in the amount of retained hydrocarbons does not necessarily mean that the amount of carbon-containing deposits decrease; on the opposite, it has previously been found that a decrease in the amount of retained hydrocarbons is often accompanied by an increasing amount of insoluble coke [25]. Moreover, since hydrocarbon residues were only analysed at the end of each test, we are not in position to elucidate whether catalyst deactivation is correlated with internal or external coke formation.

3.2.2 Catalytic Testing of H-ITQ-13(P) at Ambient Pressure H-ITQ-13(P) differs from H-ITQ-13(N) with respect to morphology (sheet-like versus needle-like) and acid site density ((Al below quantification limit versus (Si+Ge)/ Al = 42), but the two materials have similar specific surface area and acid strength (Sect. 3.1). Conversion versus time on stream data for H-ITQ-13(P) at 400 C° and WHSV = 2 h-1 are shown in Fig. 6 above (Sect. 3.2.1), together with the corresponding data for H-ITQ-13(N). A lower initial conversion was observed over H-ITQ- 13(P) compared to H-ITQ-13(N) (70 vs. 97 %, respectively), in line with the lower density of acid sites in H-ITQ-13(P) (Sect. 3.1). Only modest deactivation of H-ITQ-13(P) was observed during the test duration of 95 h, suggesting that this material would yield a higher methanol conversion capacity than H-ITQ-13(N). Similar behavior was previously observed for methanol conversion over mordenite with Si/Al ratios in the range of 5–103 [36]. Differences in lifetime with respect to differences in acid site densities can be explained by the higher number of successive chemical steps undergone by reactants in samples with short distances between the acid sites and the tendency to favour condensation reactions which both increase the coking rate [5].

3.2.3 Comparison of H-ITQ-13(P) and H-ITQ-13(N)

Detailed gas chromatograms of the reactor effluent obtained over the two materials at 70 % conversion at 400 C° are shown in Fig. 10. Isobutane, isobutene, trans-2-butene and cis-2-butene were represented among the C4 fraction. n-Butane was also present, but only in small quantities. Benzene, toluene, xylenes and trimethylbenzenes were detected and the latter was the most dominating among the aromatics. The largest aromatic compound identified was tetramethylbenzene,but the quantity was negligible. The selectivity to various product groups over

the two materials is shown in Fig. 7 above (Sect. 3.2.1) and quantified for two conversion levels (58 and 70 %) in Table 1.

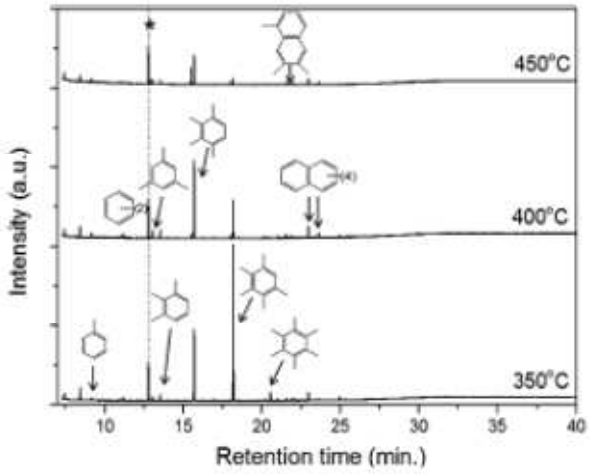

Fig. 9 Retained species in H-ITQ-13(N) after dissolution of the zeolite and extraction of the organic phase at the end of the experiments. The symbol asterisk is indicating the internal standard

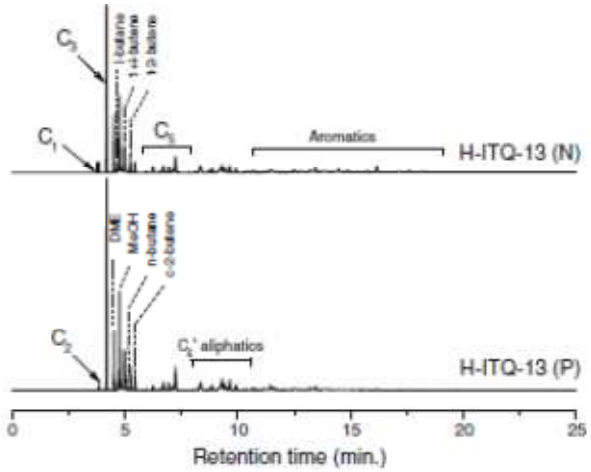

Fig. 10 Gas chromatograms of the product effluent showing the selectivity at 70 % conversion over H-ITQ-13(N) (upper curve) and H-ITQ-13(P) (lower curve), respectively. Temperature = 400 C°, WHSV = 2 h-1; time on stream for H-ITQ-13(N) is 62 h and for H-ITQ-13(P) 5 min

Table 1 Selectivity of H-ITQ-13(N) and (P) at comparable conversions (70 and 58 %). The reaction was performed at 400 °C and WHSV = 2 h^{-1}

Catalyst	Conversion (%)	C_1	C_2	C_3	C_4=	C_4–	C_5	C_{6+} aro.	C_{6+} ali.
H-ITQ-13(N)	70	1.5	1.8	28	16	3.3	14	6.1	29
	58	1.8	1.7	27	16	2.8	14	6.2	31
H-ITQ-13(P)	70	0.1	0.9	30	19	2.1	14	2.3	32
	58	0.2	0.7	28	19	1.3	14	2.1	35

The global selectivity pattern was similar for the two materials, with C6+ aliphatics and C3 being the main products over both materials, followed by C4 alkenes and C5. The main difference between the materials was the methane selectivity, which was one order of magnitude higher over H-ITQ-13(N) than over H-ITQ-13(P) (2 vs. 0.2 %, respectively). No straightforward explanation has been found to this observation, although a correlation between deactivation level and methane selectivity was observed (See Fig. S8 in Supporting Information). Furthermore, the selectivity to C6+ aromatics was 3 times higher over H-ITQ-13(N) than over H-ITQ-13(P) (6 vs. 2 %, respectively) and the ethene selectivity was two times higher over H-ITQ-13(N) than over H-ITQ-

13(P) (1.7 vs. 0.7 %, respectively). It is noteworthy that the propene to ethene ratio obtained over H-ITQ-13(P) was very high; between 34 and 41 in the conversion range tested (58–70 % conversion), versus 16 for H-ITQ-13(N). The observed differences in aromatics and ethene selectivities are in line with previous literature concerning other topologies (MOR and MFI) as MTH catalysts, where it was reported that a lower acid site density and a smaller MFI crystal size would favor alkenes over aromatic products, and propene over ethene (See Sect. 1.1) [31–33, 35, 36]. It is not straightforward to allocate the observed activity and selectivity differences between H-ITQ-13(N) and H-ITQ-13(P) to a single material parameter, since their two main differences; a lower density of acid sites and a shorter diffusion pathway in H-ITQ-13(P), are both expected to alter the effluent selectivities in the same direction (See Sect. 1.1). In a possible search for optimised propene yields, a sheet-like morphology may however be a key parameter: As referred to in the Sect. 1.1, similar propene to ethene ratios to those obtained here over H-ITQ- 13(P) have previously been obtained for H-ZSM-5 with nanosheet morphology [34]. A third parameter which may influence product selectivity is lattice defects: A study [59] comparing H-ZSM-5 samples having different amounts of Al- and Si-defects showed that even low concentration of Al- and Si-related defective sites could substantially affect the product composition during the MTH reaction. Lowdefective, highly ordered H-ZSM-5 favoured formation of C2 and C3 alkenes on the account of C1–C4 paraffins and aromatics. Furthermore, an increased coking rate was observed for micro mesoporous H-ZSM-5 which had defective Al- and Si- sites. Hence defects may alter both the selectivity and deactivation rate. As evident from FTIR data, both materials, H-ITQ-13(N) and (P) contained defective sites. However it was difficult to quantify the number of defects in these materials based on available characterisation, and we may only state that an additional influence of such defect sites on product selectivity cannot be excluded.

3.2.4 Catalytic Testing of H-ITQ-13(N) at High Pressure (30 bar)

Catalytic test data for H-ITQ-13(N) at 350 C° and 1 and 30 bar pressure (P(CH3OH) = 0.13 and 1.7 bar, respectively) are shown in Fig. 11. Elevated pressure was expected to lead to an increase in C5+ product selectivity since C–C formation is facilitated at high pressure. Reactionscarried out at 350 C°, WHSV = 2 h-1 and P = 30 bar showed full conversion for 5 h before rapid and stable deactivation started. Low pressure tests at similar conditions did not lead to full conversion (about 90 %) and after reaction onset the sample showed stable deactivation.At 40 % conversion the catalyst tested at low pressure had been on stream for around 60 h, 47 h more than for the same conversion at high pressure. Extrapolation of the conversion versus time on stream curves in Fig. 11 indicated an almost ten-fold decrease in methanol conversion capacity at the higher pressure. At low pressure C3 selectivity between 20 and 25 % was obtained in a wide range of conversions (90–30 %) as shown in Fig. 11. When performing the same experiment at high pressure, the selectivity towards C3 decreased to 5–11 % and the selectivity for C5+ was increased. For all data pointscollected at high pressure, the gasoline fraction, i.e.; C5+ hydrocarbons, represented between 65 and 70 % of the effluent products and was clearly more dominating than in the low pressure tests. Furthermore, much more aromatics were formed at high pressure; giving 15–30 % aromaticsselectivity. In agreement with the formation of saturated hydrocarbons at high pressure, a higher hydrogen transfer index (HTI), defined as the ratio between the amount of C4 alkanes and the amount of C4 alkenes and alkanes combined, was found for the sample tested at high

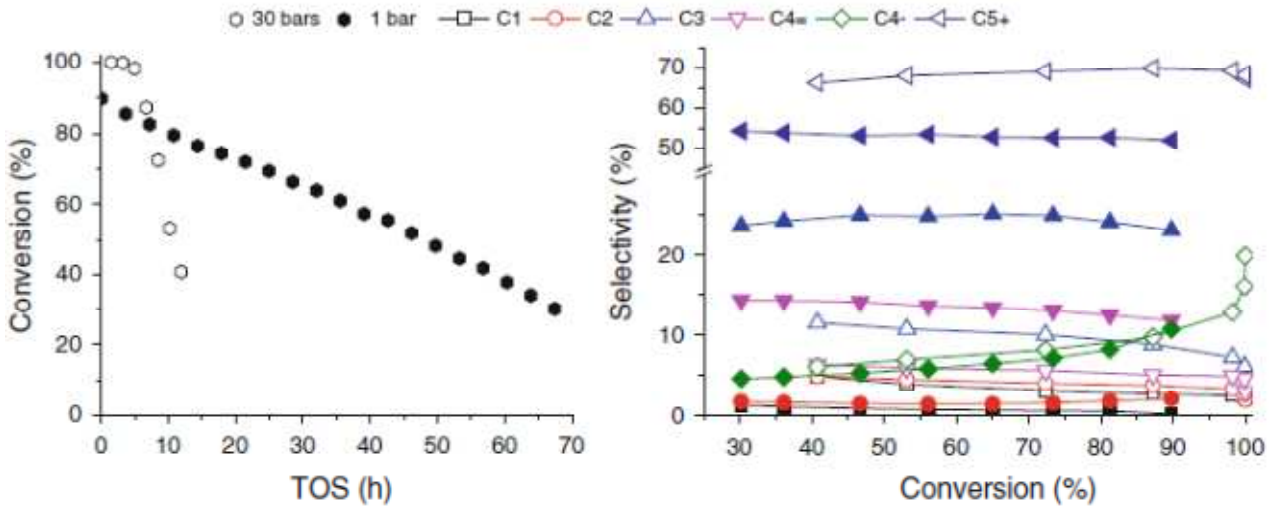

Fig. 11 Left panel conversionversus TOS (h) at ambient (closed symbols) and high pressure (30 bar) (open symbols) at 350 C° and WHSV = 2 h-1. Right panel selectivity versus conversion for high pressure (open symbols) and ambient pressure (closed symbols)

Table 2 Main characteristics of investigated catalysts (For further details we refer to Sect. S.1 in Supporting Information)

Sample	Main characteristics of the investigated catalysts					
	Si/Al	ΔOH [cm^{-1}][d]	Surface $area_{BET}$ [m^2/g]	Micropore/mesopore volume [cm^3/g]	Particle shape	Particle size
H-ITQ-13(N)	42[a]	−327 (310)	413	0.15/0.09	Needles	<3 μm × 100 nm
H-ITQ-13(P)	>100[a]	−(~327)	455	0.15/0.54	Plate-like	Typically 1 μm in the longest direction
H-ZSM-22	50[b]/48[c]	−316	197	0.07/0.07	Rods	Typically 1–3 μm length
H-ZSM-5	49[a]/50[b]	−303	430	0.16/0.10	Elliptical	<5 μm, typically <2.5 μm

[a] EDS
[b] Supplier
[c] TPD
[d] Brønsted band

Based on the test referred to above, the methanol conversion capacity for the three catalysts was calculated to 6.5 g g-1 catalyst for H-ZSM-22, *140 g g-1 catalyst for H-ITQ-13(N) and *520 g g-1 catalyst for H-ZSM-5 (Fig. S7, Supporting Information). It should be noted that the H-ZSM-5 catalyst was so stable that the WHSV was changed to 9 h-1 after *70 h on stream in order toaccelerate deactivation. Coke formation is a main reason for catalyst deactivation in MTH. A comparison of retine hydrocarbons reported for H-ITQ-13(N) in this study (Fig. 9) and those reported previously for H-ZSM-5 [25] and H-ZSM-22 [61] after deactivation showed significant differences between H-ZSM-5 and the two more narrowpored zeolites, in agreement with the superior methanol conversion capacity of H-ZSM-5: H-ZSM-5 contained only monocyclic aromatics after testing, and no correlation was found between the amount of retained aromatics and deactivation [25]. H-ZSM-22 contained mono-, di- and tricicli aromatic molecules after testing [61], while H-ITQ-13(N) contained mono- and bicyclic aromatics as well as traces of tricyclic aromatics (Fig. 9). Concentrating first on the difference between the 3-dimensional channel structures of H-ZSM-5 and H-ITQ-13, similar results have previously been reported for the 3-dimensional (3D) ten-ring structures H-TNU-9 and H-IM-5, compared to 3D ten-ring H-ZSM-5 and -11: while H-TNU- and H-IM-5 contained polycyclic aromatic compounds after testing, H-ZSM-5 and -11 contained only monocyclic aromatic compounds [51]. The difference wasallocated to the presence of spacious intersection volumes in the two first structures compared to the two latter [51]. Similarly, in H-ITQ-13 a larger space is present at thechannel intersections compared to H-ZSM-5: The intersectionsof H-ITQ-13 are big enough to entrap a sphere of 6.72 A ° diameter, which is significantly larger than

the sphere that can be entrapped within H-ZSM-5 (6.36 A°).The methanol conversion capacity of H-ITQ-13 was 20 times higher than that of H-ZSM-22 (Figure S7). Due to the

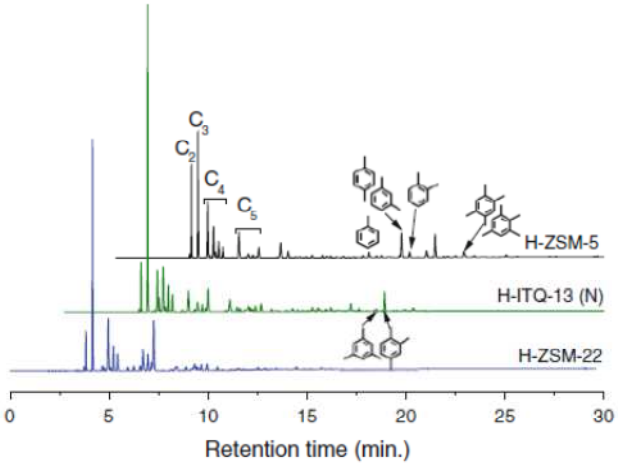

Fig. 12 Gas chromatograms obtained over H-ZSM-22, H-ITQ- 13(N) and H-ZSM-5, respectively, at 400 C° and WHSV = 2 h-1 at full conversion (97 % conversion for H-ITQ-13(N))

similar channel sizes of these two materials, the most probable reason for this difference is the 3D channel system of H-ITQ-13, combined with a needle-like morphology with short diffusion pathways in two directions (Table 2), compared to the 1D channel system of H-ZSM-22. Detailed gas chromatograms of the effluent from H-ZSM-5, H-ZSM-22 and H-ITQ-13(N) at full methanol conversion at 400 C° are shown in Fig. 12. It is evident from Fig. 12 that the product cut-off was similar for H-ZSM-5 and H-ITQ-13, with tetraMB as the largest significant product, and only traces of higher polyMBs. H-ZSM-22 on the other hand, produced mainly linear and branched alkenes, while only traces of aromatic products could be observed. The ability of H-ITQ-13 to yield aromatic products in the effluent was surprising, taking into account that its channel dimensions are inferior to the single channel of H-ZSM-22. It has previously been shown that even H-ZSM-22 produces small amounts of aromatic molecules; however, those products are trapped inside the channels and lead to catalyst deactivation [61]. H-ZSM-48, another 1-dimensional ten-ring structure with slightly larger channelsthan H-ZSM-22, i.e. 5.3 9 5.6 A ° , has been shown to yield aromatic products even in the effluent, although to a smaller extent than H-ZSM-5 [56]. Several possible explanations exist for the observed difference in product cut-of between H-ITQ-13 and H-ZSM-22: One possibilityis that the subtle difference in pore size between the tested materials is outweighed by e.g. a more pronounced pore breathing of the less dense H-ZSM-5 and H-ITQ-13 materials compared to the denser H-ZSM-22 material (19.7 vs. 17.9 and 17.8 T-atoms per 1,000 A ° 3, respectively). A higher production of aromatic species in the intersections of H-ZSM-5 and H-ITQ-13 materials compared to the unidimensional H-ZSM-22 (see below) would further contribute to a strong potential for diffusion via pore breathing. Another possibility is exposure of canne intersections to the outer surface of the H-ITQ-13 catalyst, leading to formation of heavier products there. Such a phenomenon has previously been suggested for H-EU-1, which has a 1-dimensional structure with narrow channels (4.1 9 5.4 A °) but large side-pockets, and which produces aromatic products to a significant extent [56]. A comparison between product selectivities for H-ITQ-13(N), H-ITQ-13(P), H-ZSM-5 and H-ZSM-22 as a function of methanol conversion at 400 C° is shown in Fig. 13. We will first compare H-ITQ-13(N) with the two materials with different topology. Considering first the two main product fractions, C5+ and C3 (right panel), H-ITQ-13(N) gave slightly lower propene selectivities than H-ZSM-5, and slightly higher C5+ selectivities than H-ZSM-5, whereas H-ZSM-22 gave much higher C5+ selectivities, and lower C3 selectivities, than the two other materials. Concerning the HTI (i.e. the sum of C4 alkanes divided by the sum of C4 alkanes and C4 alkenes) (Fig. 13, left panel), H-ITQ- 13(N) was closer to H-ZSM-5 than to H-ZSM-22, in

accordance with its effluent selectivity to aromatic products, which was also intermediate between the two (Fig. 12). It is of interest to discuss the observations in Fig. 13 with respect to the dual-cycle reaction mechanism, which is illustrated in Scheme 1. According to this mechanism, the MTH reaction is a sequential reaction, starting with production of light alkenes, which may subsequently be methylated to form higher alkenes, and, thereafter, possibly form aromatics and alkanes by intermolecular hydrogen transfer. The aromatic products may in their turn be methylated and subsequently form alkenes by dealkylation reactions. These alkenes may again be converted to higher alkenes and aromatics/alkanes by reactions already described. As such, all alkenes and (monocyclic) aromatic compounds are considered as reaction centers as well as products, and the effluent concentration of each compound depends on the relative rate of each individual reaction over the selected catalyst. When considering a catalyst's ability to form aromatic products, it is useful to monitor its C4 HTI, which represents intermolecular hydrogen transfer reactions, based onproducts which may easily diffuse out of all structures considered here. From Fig. 13, it appears that H-ZSM-22, with its 1D ten-ring channels, had a much lower ability to form aromatic products than H-ITQ-13 and, especially, H-ZSM-5, which both contain more spacious canne intersections. Aromatisation thus appears to be spatially hindered in H-ZSM-22. Interestingly, H-ITQ-13(P), with sheet-like morphology and much lower density of acid sites compared to the other samples, gave similar C4 HTI to H-ZSM-22. We ascribe this observation to a lower tendency of sequential reactions in the channels of H-ITQ-13(P). Another main difference between H-ZSM-22 and either of H-ITQ-13((N) and (P)) and H-ZSM-5, is the high C5+ selectivity obtained over H-ZSM-22 (Fig. 13, right panel). This observation suggests that even alkene cracking reactions are spatially hindered in H-ZSM-22 compared to alkene methylation reactions, thereby altering the steady state product concentrations in the direction of the heavier alkenes. H-ITQ-13(N) and H-ZSM-5 gave similar C3 selectivity, but H-ZSM-5 gave a slightly higher C4-HTI, and slightly lower C5+ selectivity, than H-ITQ-13(N).This observation may suggest that the more spatially demanding intermolecular hydrogen transfer reactions, but not alkene cracking reactions, proceed more slowly compared to alkene methylation reactions in H-ITQ-13(N) than in H-ZSM-5. As a final observation, the propene to ethene ratio (Fig. 13, left panel), was higher over H-ITQ-13, and especially over H-ITQ-13(P), than over the other materials. As referred to in the Sect. 1.1, ethene formation is generally related to the aromatics-based hydrocarbon pool cycle. As such, the higher C3/C2 ratio observed over H-ZSM-22 compared to H-ZSM-5 has previously been ascribed to a lesser abundance of the aromatics cycle in H-ZSM-22 [27].

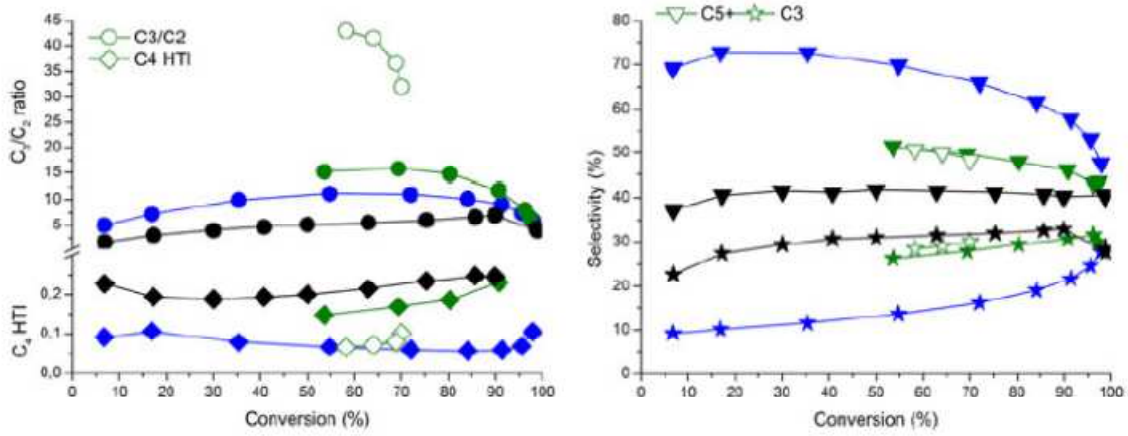

Fig. 13 Comparison of critical parameters of the two different H-ITQ-13 samples, H-ZSM-22 and H-ZSM-5 at 400 C° and WHSV = 2 h-1. The C3/C2 ratio and the C4 HTI are shown in the left panel, while the selectivity towards C3 and C5+ is shown in the right panel. Blue symbols ZSM-22, closed green symbols H-ITQ-13(N), green open symbols H-ITQ-13(P) and black symbols H-ZSM-5. Because H-ZSM-5 showed very slow deactivation the WHSV was changed from 2 to 9 h-1 after 70 h on stream. Thus for H-ZSM-5 the first point at maximum conversion is measured at WHSV = 2 h-1 and the subsequent points at 9 h-1.

In the present case, the rather large channel intersections in H-ITQ-13, as well as the higher C4 HTI and high selectivity to C3-C4 alkenes over H-ITQ-13 compared to H-ZSM-22, are all indications of a more active aromatics cycle in H-ITQ-13 compared to H-ZSM-22. We are not in position to explain the observed, low selectivity to ethene over the H-ITQ-13 catalysts. One might speculate that the aromatics fraction present in H-ITQ-13 has a lower selectivity to ethene than that present in H-ZSM-5, due to a different intersection volume. Comparative studies of H-ZSM-5 and H-Beta zeolite have previously shown that over H-ZSM-5, the lower methylbenzenes which are dominating hydrocarbon pool species lead to formation of ethene and propene. Over H-beta catalysts, the higher methylbenzenes dominate and produce mainly propene and isobutane [23]. Under comparative reaction conditions, H-Beta (Si/Al = 120) produced a C3/C2 ratio of 21 at 55 % conversion, while H-ZSM-5 (Si/Al = 140) catalyst produced a C3/C2 ratio 3.1 at 73 % conversion [23]. However, the knowledge about ethene conversion reactions under MTH conditions is still limited, and any conclusion on this subject would be premature.

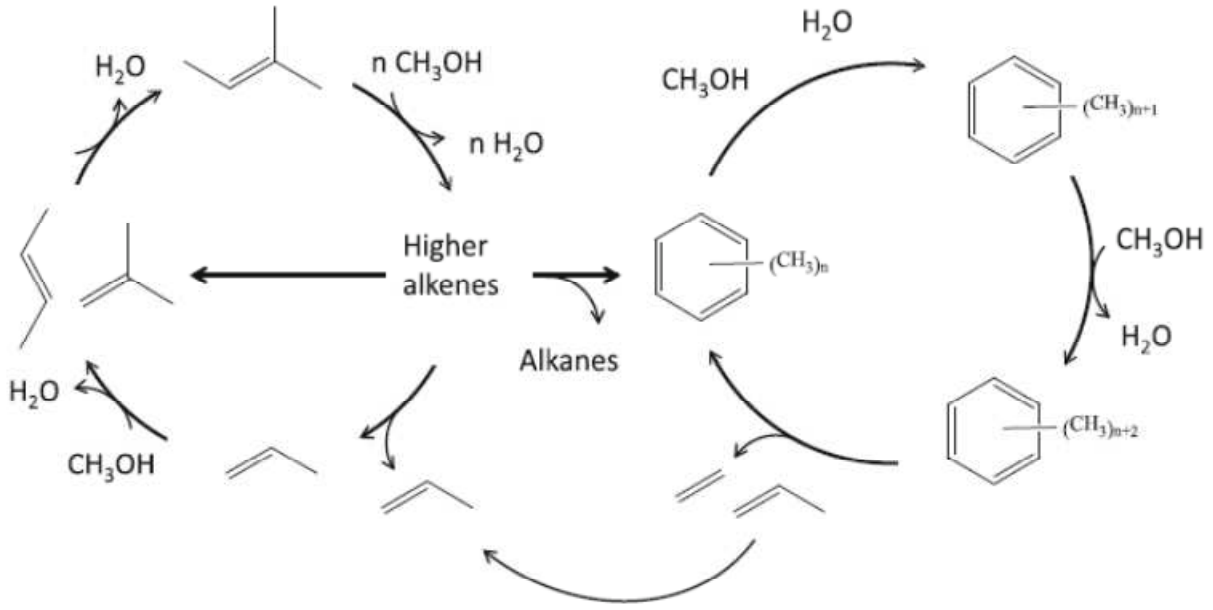

Scheme 1 The dual-cycle mechanism. Adapted from [5]

4 Conclusion

H-ITQ-13 was found to be an active catalyst for the (MTH) reaction. Two samples which differed in acid site density and morphology (needles and plates) were compared and produced mainly C3 and C6+ aliphatics in the effluent stream. The sample with low acid site density yielded a much higher propene to ethene ratio (34–41 under conditions tested compared to 16) and gave less aromatics (2 % aromatics) in the effluent than the sample with higher acid site density (6 % aromatics). Under high pressure conditions the C5+ fraction was enhanced from about 55 to 65–70 %. However much more aromatics was formed under pressurised conditions followed by a close to ten-fold drop in the total conversion capacity compared to ambient pressure conditions. Under ambient pressure conditions H-ITQ-13 yielded a product spectrum intermediate of H-ZSM-5 and H-ZSM-22. Surprisingly H-ITQ-13 gave the same cut-off in the effluent stream as H-ZSM-5 despite an inferior canne size compared to H-ZSM-22 which showed mainly linear and branched alkenes in the effluent. The stability of the herein tested H-ITQ-13 materials was clearly lower than H-ZSM-5, but substantially higher than that of H-ZSM-22, both with similar density and strength of acid sites as H-ITQ-13. The total conversion capacity of H-ITQ-13 was in the range of 120–150 g methanol g-1 of catalyst, while the H-ZSM-22 sample had a total conversion capacity of 6.5 g methanol g^{-1} of

catalyst and the H-ZSM-5 sample a total conversion capacity of *520 g methanol per gram of catalyst under the conditions tested. The main aim of this study was to gain further flexibility in the product spectrum of the methanol to hydrocarbon process as the market is not fixed. From this perspective H-ITQ-13 fills one hole in the product spectrum library yielded from the large range of known and hypothetical predicted shape selective zeolite catalysts.

References

1. Shell, http://www.shell.com/home/content/innovation/meeting_demand/natural_gas/gtl/. Accessed 30 March 2012
2. Chang CD, Silvestri AJ (1977) J Catal 47:249–259
3. Sto¨cker M (1999) Microporous Mesoporous Mater 29:3–48
4. Haw JF, Song WG, Marcus DM, Nicholas JB (2003) Acc Chem Res 36:317–326
5. Olsbye U, Svelle S, Bjørgen M, Beato P, Janssens TVW, Joensen F, Bordiga S, Lillerud KP (2012) Angew Chem Int Ed 51; 5810–5831
6. Chen NY, Reagan WJ (1979) J Catal 59:123–129
7. Dahl IM, Kolboe S (1993) Catal Lett 20:329–336
8. Dahl IM, Kolboe S (1994) J Catal 149:458–464
9. Dahl IM, Kolboe S (1996) J Catal 161:304–309
10. Song WG, Marcus DM, Fu H, Ehresmann JO, Haw JF (2002) J Am Chem Soc 124:3844–3845
11. Lesthaeghe D, Van Speybroeck V, Marin GB, Waroquier M (2006) Angew Chem Int Ed 45:1714–1719
12. Wragg DS, O'Brien MG, Bleken FL, Di Michiel M, Olsbye U, Fjellvag H (2012) Angew Chem Int Ed 51:7956–7959
13. White JL (2011) Catal Sci Technol 1:1630–1635
14. Smit B, Maesen TLM (2008) Chem Rev 108:4125–4184
15. Arstad B, Kolboe S (2001) J Am Chem Soc 123:8137–8138
16. Arstad B, Kolboe S (2001) Catal Lett 71:209–212
17. Song WG, Haw JF, Nicholas JB, Heneghan CS (2000) J Am Chem Soc 122:10726–10727
18. Sassi A, Wildman MA, Ahn HJ, Prasad P, Nicholas JB, Haw JF (2002) J Phys Chem B 106:2294–2303
19. Bjørgen M, Olsbye U, Petersen D, Kolboe S (2004) J Catal 221: 1–10
20. Svelle S, Rønning PO, Kolboe S (2004) J Catal 224:115–123
21. Svelle S, Rønning PO, Olsbye U, Kolboe S (2005) J Catal 234: 385–400
22. Bjørgen M, Akyalcin S, Olsbye U, Benard S, Kolboe S, Svelle S (2010) J Catal 275:170–180
23. Bjørgen M, Joensen F, Lillerud KP, Olsbye U, Svelle S (2009) Catal Today 142:90–97
24. Svelle S, Joensen F, Nerlov J, Olsbye U, Lillerud KP, Kolboe S, Bjørgen M (2006) J Am Chem Soc 128:14770–14771
25. Bjørgen M, Svelle S, Joensen F, Nerlov J, Kolboe S, Bonino F, Palumbo L, Bordiga S, Olsbye U (2007) J Catal 249:195–207
26. Svelle S, Olsbye U, Joensen F, Bjørgen M (2007) J Phys Chem C 111:17981–17984
27. Teketel S, Olsbye U, Lillerud KP, Beato P, Svelle S (2010) Microporous Mesoporous Mater 136:33–41
28. Topp-Jørgensen J (1988) Stud Surf Sci Catal 36:293–305
29. Kvisle S, Nilsen HR, Fuglerud T, Grønvold A, Pujado PR, Barger PT, Andersen JM (2002) Abstr Pap Am Chem Soc 223:U648
30. Kvisle S, Fuglerud T, Olsbye U, Lillerud KP, Vora BV (2008) Methanol-to-hydrocarbons. In: Ertl G, Knozinger H, Weitkamp J
(eds) Handbook of heterogeneous catalysis. Wiley-VCH Verlag
GmbH, Weinheim, pp 2950–2965
31. Chang CD, Chu CTW, Socha RF (1984) J Catal 86:289–296
32. Chu CTW, Chang CD (1984) J Catal 86:297–300
33. Prinz D, Riekert L (1988) Appl Catal 37:139–154
34. Beken BTL, Wragg DS, Arstad B, Gunnæs AE, Mouzon J,
Helveg S, Lundegaard LF, Beato P, Bordiga S, Svelle S, Olsbye
U, Lillerud KP (2013) Top Catal (in press)
35. Lønstad Bleken F, Chavan S, Olsbye U, Boltz M, Ocampo F, Louis B (2012) Appl Catal A 447–448:178–185
36. Park JW, Kim SJ, Seo M, Kim SY, Sugi Y, Seo G (2008) Appl Catal A 349:76–85
37. International Zeolite Association, http://www.iza-online.org. Accessed 12 Dec 2012
38. Corma A, Jiang JX, Yu JH (2010) Angew Chem Int Ed49:3120–3145

39. Castaneda R, Corma A, Fornes V, Martinez-Triguero J, Valencia S (2006) J Catal 238:79–87
40. Boix T, Puche M, Camblor MA, Corma A (2002) US 6,471,941 B1, to ExxonMobil Research and Engineering Company
41. Sastre G, Pulido A, Castaneda R, Corma A (2004) J Phys Chem 108:8830–8835
42. Corma A, Diaz-Cabanas MJ, Jiang J, Afeworki M, Dorset DL, Soled SL, Strohmaier KG, Natl P (2010) Acad Sci USA 107:13997–14002
43. Petkov PS, Aleksandrov HA, Valtchev V, Vayssilov GN (2012) Chem Mater 24:2509–2518
44. Jiang JX, Jorda JL, Diaz-Cabanas MJ, Yu JH, Corma A (2010) Angew Chem Int Ed 49:4986–4988
45. Vidal-Moya JA, Blasco T, Rey F, Corma A, Puche M (2003) Chem Mater 15:3961–3963
46. Sastre G, Vidal-Moya JA, Blasco T, Rius J, Jorda JL, Navarro MT, Rey F, Corma A (2002) Angew Chem Int Ed 41:4722–4726
47. Kosslick H, Tuan VA, Fricke R, Peuker C, Pilz W, Storek W (1993) J Phys Chem 97:5678–5684
48. Skorpa R, Bordiga S, Bleken F, Olsbye U, Arstad B, Tolchard J, Mathisen K, Svelle S, Bjørgen M (2011) Microporous MesoporousMater 141:146–156
49. Leiva S, Sabater MJ, Valencia S, Sastre G, Fornes V, Rey F, Corma A (2005) Cr Chim 8:369–378
50. Gribov EN, Cocina D, Spoto G, Bordiga S, Ricchiardi G, Zecchina A (2006) Phys Chem Chem Phys 8:1186–1196
51. Bleken F, Skistad W, Barbera K, Kustova M, Bordiga S, Beato P, Lillerud KP, Svelle S, Olsbye U (2011) Phys Chem Chem Phys 13:2539–2549
52. Bjørgen M, Lillerud KP, Olsbye U, Bordiga S, Zecchina A (2004) J Phys Chem B 108:7862–7870
53. Mikkelsen Ø, Kolboe S (1999) Microporous Mesoporous Mater 29:173–184
54. Schulz H (2010) Catal Today 154:183–194
55. Bleken FL, Janssens TVW, Svelle S, Olsbye U (2012) Microporous Mesoporous Mater 164:190–198
56. Teketel S, Skistad W, Benard S, Olsbye U, Lillerud KP, Beato P, Svelle S (2012) ACS Catal 2:26–37
57. Janssens TVW (2009) J Catal 264:130–137
58. Kumar P, Thybaut JW, Teketel S, Svelle S, Beato P, Olsbye U, Marin GB (2013) Catal Today 215:224–232
59. Sazama P, Wichterlova B, Dedecek J, Tvaruzkova Z, Musilova Z,Palumbo L, Sklenak S, Gonsiorova O (2011) Microporous Mesoporous Mater 143:87–96
60. Hayasaka K, Liang D, Huybrechts W, De Waele BR, Houthoofd KJ, Eloy P, Gaigneaux EM, vanTendeloo G, Thybaut JW, Marin GB, Denayer JFM, Baron GV, Jacobs PA, Kirschhock CEA, Martens JA (2007) Chem Eur J 13:10070–10077
61. Teketel S, Svelle S, Lillerud KP, Olsbye U (2009) ChemCat-Chem 1:78–81